3. K. Towe, *Science* **157**, 1048 (1967).
4. D. M. Raup, *J. Geol.* **67**, 661 (1959).
5. S. Weiner, L. Addadi, H. Wagner, *Mater. Sci. Eng.* **11**, 1 (2000).
6. S. Loven, *Sven. Vetensk. Akad. Handl.* **18**, 1 (1892).
7. W. B. Carpenter, *Brit. Assoc. Adv. Sci. London Rep.* **17**, 93 (1847).
8. K. Okazaki, *Embryologia (Nagoya)* **5**, 283 (1960).
9. J. B. Pilkington, *J. Mar. Biol. Assoc. UK* **49**, 857 (1969).
10. K. Märkel, U. Röser, *Zoomorphology* **103**, 25 (1983).
11. K. Märkel, U. Röser, M. Stauber, *Zoomorphology* **109**, 79 (1989).
12. F. H. Wilt, *Zool. Sci.* **19**, 253 (2002).
13. E. Beniash, J. Aizenberg, L. Addadi, S. Weiner, *Proc. R. Soc. London B Biol. Sci.* **264**, 461 (1997).
14. E. Beniash, L. Addadi, S. Weiner, *J. Struct. Biol.* **125**, 50 (1999).
15. I. M. Weiss, N. Tuross, L. Addadi, S. Weiner, *J. Exp. Zool.* **293**, 478 (2002).
16. K. Märkel, U. Röser, *Zoomorphology* **103**, 43 (1983).
17. B. M. Heatfield, *J. Exp. Zool.* **178**, 233 (1971).
18. P. Dubois, C. P. Chen, *Echinoderm Stud.* **3**, 109 (1989).
19. P. Dubois, L. Ameye, *Microsc. Res. Tech.* **55**, 427 (2001).
20. L. Brecevic, N. A. *J. Cryst. Growth* **98**, 504 (1989).
21. F. Lippmann, *Sedimentary Carbonate Minerals* (Springer, Berlin, 1973).
22. Materials and methods are available as supporting material on *Science* Online.
23. L. Addadi, S. Raz, S. Weiner, *Adv. Mat.* **15**, 959 (2003).
24. S. Raz, P. C. Hamilton, F. H. Wilt, S. Weiner, L. Addadi, *Adv. Funct. Mater.* **13**, 480 (2003).
25. A. Berman, L. Addadi, S. Weiner, *Nature* **331**, 546 (1988).
26. G. F. Xu, N. Yao, I. A. Aksay, J. T. Groves, *J. Am. Chem. Soc.* **120**, 11977 (1998).
27. J. Aizenberg, J. L. Grazul, D. A. Muller, D. R. Hamann, *Science* **299**, 1205 (2003).
28. L. B. Gower, D. J. Odom, *J. Cryst. Growth* **4**, 719 (2000).
29. E. Loste, F. C. Meldrum, *Chem. Commun.*, 901 (2001).
30. We thank M. Cohen for help with the ESEM measurements. We also thank B. Scharfstein, I. Ivry, and Y. Raz (SeaOr Marine Enterprises Ltd.) for providing the animals and facilities for spine regeneration. L.A. is the incumbent of the Dorothy and Patrick Gorman Professorial Chair of Biological Ultrastructure, and S.W. is the incumbent of the Dr. Trude Burchardt Professorial Chair of Structural Biology. Supported by a grant from the Philip Klutznick Research Fund.

Earth Tides Can Trigger Shallow Thrust Fault Earthquakes

Elizabeth S. Cochran,[1]* John E. Vidale,[1] Sachiko Tanaka[2]†

We show a correlation between the occurrence of shallow thrust earthquakes and the occurrence of the strongest tides. The rate of earthquakes varies from the background rate by a factor of 3 with the tidal stress. The highest correlation is found when we assume a coefficient of friction of $\mu = 0.4$ for the crust, although we see good correlation for μ between 0.2 and 0.6. Our results quantify the effect of applied stress on earthquake triggering, a key factor in understanding earthquake nucleation and cascades whereby one earthquake triggers others.

For more than a century, researchers have sought to detect the effect on the timing of earthquakes of the gravitational perturbations on Earth from the Moon and Sun (*1*). However, the tidal stresses in most locations are small, and usually it is difficult to ascertain the orientation of the fault plane, which is critical when calculating the effect of the stress variations. Earthquake-tide correlations have been observed to be small or nonexistent in normal crust (*2–4*); however, correlations have been shown in shallow, possibly hydrothermal or magma-related areas (*5*, *6*). Here, we take advantage of accurate accounting of ocean tides (*7*) and a large data set of earthquake focal mechanisms with fairly well known fault planes (*8*) to look for a correlation.

We used global earthquakes in the Harvard Centroid Moment Tensor (CMT) catalog (*9*). For each event, we calculated a tidal-stress time series that includes the solid Earth tide and an ocean-loading component (*7*, *10*, *11*). Solid-Earth tides induce stresses only up to 5×10^3 Pa (0.05 bar), whereas in ocean basins, water loading builds stresses up to nearly 5×10^4 Pa (0.5 bar). Both components must be accurately determined to fully resolve tidal influences on the initiation of earthquakes globally. We resolved tidal stresses into normal and shear stress acting on each of the two possible fault planes of the CMT earthquake focal mechanism. Shear failure under compressive stress can be described by the Coulomb criterion, in which a fault fails under a combination of shear and normal stress: $\tau_c = \tau + \mu\sigma_n$, where τ and σ_n are the shear and normal stresses, respectively, and μ is the coefficient of friction. In addition to examining shear and normal stress independently, we tested different values of μ (0.2, 0.4, or 0.6). For each event, we calculated the tidal phase angle (θ) between $-180°$ and $180°$ (*11*); $0°$ phase is defined to be at the time of maximum stress that can promote failure, which is extensional for normal stress and in the direction of slip for shear stress (Fig. 1). In addition, we defined the average of the tidal stress amplitudes at the peaks just before and after each earthquake (τ_{pb} and τ_{pa}, respectively) to be the peak tidal stress τ_p.

We focused on a subset of shallow thrust earthquakes with depths of 0 to 40 km because these earthquakes are in regions with the
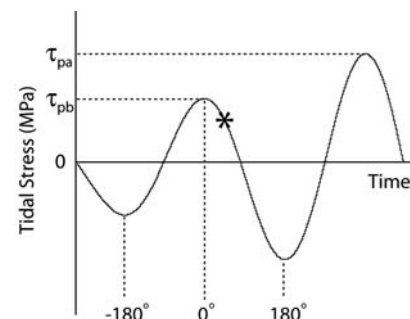
[1]Department of Earth and Space Sciences and Institute of Geophysics and Planetary Physics, University of California, Los Angeles, CA 90095, USA. [2]Department of Geophysics, Graduate School of Science, Tohoku University, Sendai, Miyagi 980-8578, Japan.

*To whom correspondence should be addressed. E-mail: cochran@moho.ess.ucla.edu
†Present address: National Research Institute for Earth Science and Disaster Prevention (NIED), Tsukuba-shi, Ibaraki-ken 305, Japan.

Fig. 1. Schematic diagram of the tidal stress time series spanning 1 day for a hypothetical earthquake (asterisk). Tidal phase is marked, with the maximum Coulomb stress promoting failure defined at $0°$ phase. The earthquake occurs at $\theta = 45°$. Peak stress amplitudes before and after an event (τ_{pb} and τ_{pa}, respectively) are averaged to determine τ_p.

Table 1. Comparison of coefficients of friction. Data are shown for the 250 events with the highest calculated tidal stress (τ_p) given different values of the coefficient of friction (μ). Binomial is approximated by a Gaussian distribution; *P* values are determined using Schuster's statistical test of data distribution (values below 5% are often considered significantly nonrandom). θ_{peak} is the phase of the peak of a sinusoidal fit to the data. See text for definition of N_{ex}.

Events	Binomial (%)	P value (%)	N_{ex} (%)	θ_{peak} (degrees)
$\mu = 0$ (shear)	4.38	10.36	5.6	−22.2
$\mu = 0.2$	0.1439	0.6253	9.6	−1.2
$\mu = 0.4$	0.0032	0.0157	12.8	0.2
$\mu = 0.6$	0.0942	0.3265	10.0	6.0
$\mu = \infty$ (normal)	0.4688	3.677	8.4	15.8

largest tidal stresses; the true fault plane is better known for these events; and shallow events are under lower confining pressures, so tidal stress may be proportionally more influential. In addition, thrust and normal faults have relatively larger tidal stress amplitudes than strike-slip faults because of a larger influence of the ocean loading component. As the ocean moves back and forth in an ocean basin, the additional weight of the water acts to clamp and unclamp dipping faults. In subduction zones, ocean loading tends to be largest and low-angle thrust events are most common. The focal mechanisms for shallow thrust faults show a bimodal distribution of fault dips for fault planes 1 and 2 (Fig. 2A). The shallower-dipping fault planes (plane 1) for the 19 events with τ_p greater than 0.02 MPa (0.2 bar) are aligned with the local geometry of the subduction zone (Fig. 2B), so for this study we assume that to be the true fault plane.

Correlation with the tides is found for shallow-dipping thrust events, assuming $\mu =$ 0.2, 0.4, or 0.6 (Fig. 3). Schuster's test, used to find statistical significance of periodicity, indicates less than a 1% probability that the distribution is random for τ_p above about 0.01 MPa (0.1 bar). More events occur during the period of encouraging stress ($-90° < \theta < 90°$) than occur during times of discouraging stress ($-180° < \theta < -90°$ or $90° < \theta < 180°$); the sinusoidal fit to the nonrandom distribution of events peaks at a tidal phase near $\theta = 0°$, which is the phase of tidal stress expected to promote failure (Fig. 4A).

We also performed a binomial test of significance because Schuster's tests may overestimate significance. We estimated the probability of seeing at random the larger fraction of earthquakes we observed to occur during the half of the tidal phase period with encouraging stress, $-90° < \theta < 90°$. If we assume that events occur at random, the number of events that occur with a tidal phase between $-90°$ and $90°$ should be equal to the number that occur in the other half of the tidal phase range. This simple binomial test gives a probability of >99.99% that earthquakes correlate with tides when tidal stress amplitudes are high (>0.01 MPa) (Fig. 3D). The binomial statistic is calculated assuming that just one choice of parameters was tested; the true odds of finding the correlation at random are expected to be somewhat lower than those obtained here. Tidal correlation with earthquake timing at the highest stress levels is apparent for most choices of coefficient of friction, but the most significant correlation is for $\mu = 0.4$ (Table 1 and Fig. 3D). Assuming $\mu = 0.4$, a minimum binomial probability of 0.0027% of fortuitous correlation (with a corresponding P value of 7.6×10^{-5} is observed for the 255 events that occur at $\tau_p > 0.003$ MPa (11).

We see fluctuations in the binomial statistics (Fig. 3D). The most highly correlated 45 events are the most highly stressed, and most are shallow, with 41 events at or above 15 km depth. The next 100 events are not as highly correlated and tend to be deeper, with only 45% of the earthquakes at
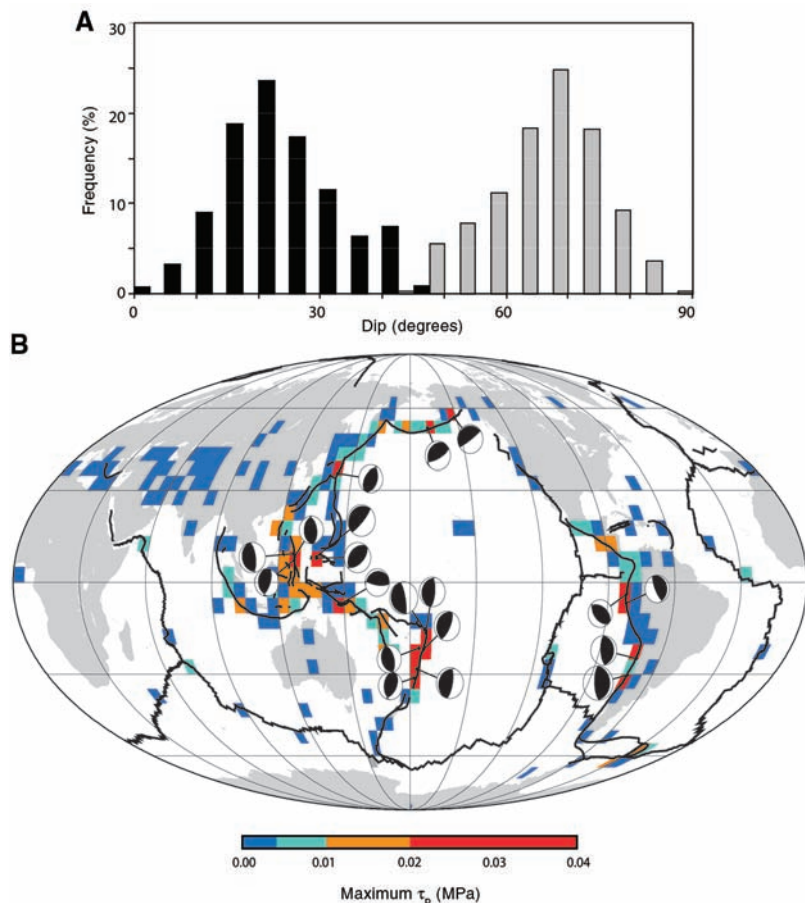

Fig. 2. (**A**) Plot of frequency versus fault dip for 2027 reverse-type earthquakes with hypocenters shallower than 40 km depth. Fault plane 1 (black) and fault plane 2 (gray) dips are from the Harvard CMT catalog focal mechanism solutions. (**B**) Global distribution of maximum τ_p assuming $\mu = 0.4$ in $5° \times 5°$ grids for all $M \geq 5.5$ global shallow thrust earthquakes. Continents are shown in light gray; plate boundaries are shown by solid black lines. Note higher peak tidal stresses (red and orange grids) at continent-ocean margins. Lower-hemisphere focal mechanisms (circular, half-filled symbols) shown for the 19 thrust events with $\tau_p \geq 0.02$ MPa agree with tectonic regime for the shallower-dipping choice of the fault plane.
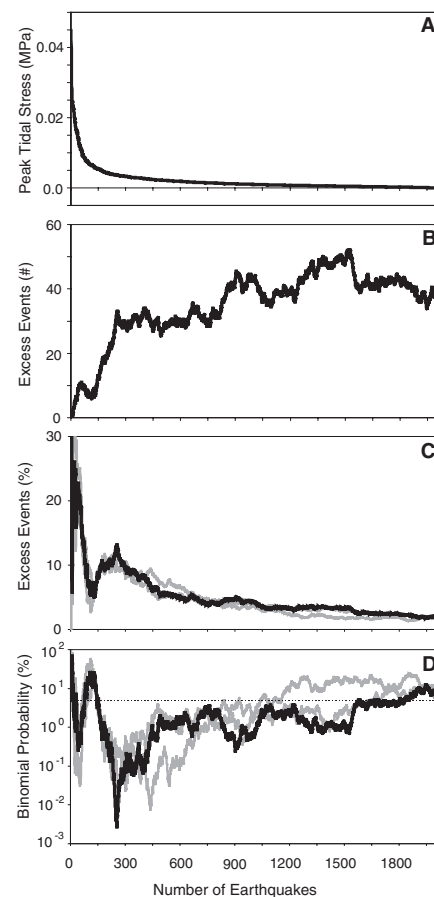
Fig. 3. (**A**) Plot of peak tidal stress τ_p versus total number of events N_{tot}. (**B**) Plot of the number of excess events N_{ex} during times of higher stress versus N_{tot}. (**C**) Plot of percentage of N_{ex} versus N_{tot}. (**D**) Binomial probability versus N_{tot} for $\mu = 0.2$ (black line), 0.4 (gray line), and 0.6 (gray line). Dashed line indicates 5% probability level for reference.

Fig. 4. (A) Histogram of frequency of events versus θ for the 255 events with the highest τ_p, assuming $\mu = 0.4$. Solid line is the sinusoidal least-squares fit to the data; dashed line is the Coulomb stress amplitude as a function of tidal phase. **(B)** Percentage of N_{ex} versus τ_p. Values are given in Table 2. Points are located at the mean τ_p; range is indicated by solid horizontal lines. Gray circles are global thrust data; solid triangle at lower left denotes California strike-slip results. Estimated SEs are shown by vertical bars. Crosses and diamonds show the least-squares fit of the data to rate- and state-dependent friction and stress corrosion, respectively.
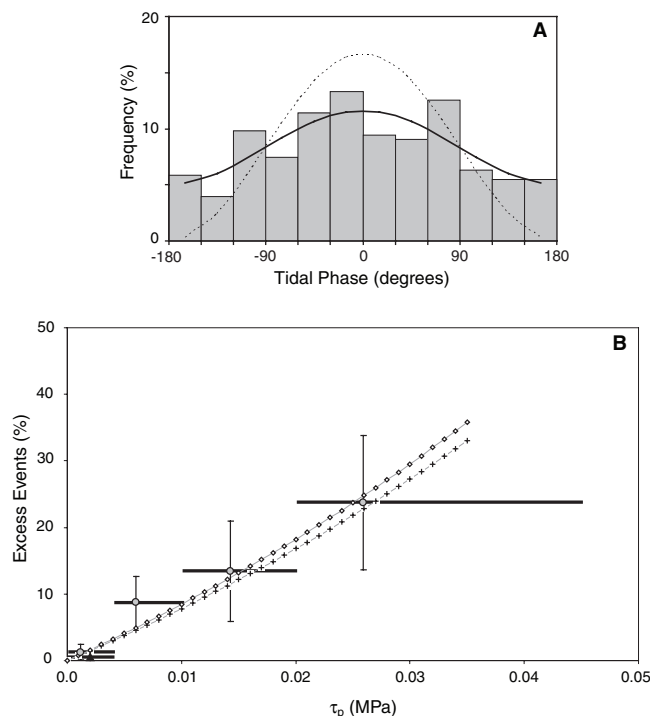
Table 2. Data summary. Both global thrust events and California strike-slip events (4) are shown for various peak Coulomb stress ranges (τ_p) given a coefficient of friction $\mu = 0.4$. N is the number of events in each τ_p bin. N_{ex} includes SE.

Data set	τ_p (MPa)	N	N_{ex} (%)
Global thrust	>0.02	19	23.7 ± 10.10
Global thrust	0.01 to 0.02	41	13.4 ± 7.52
Global thrust	0.004 to 0.01	155	8.7 ± 3.95
Global thrust	<0.004	1,813	1.2 ± 1.17
California strike-slip	<0.004	27,464	0.60 ± 0.30

or above 15 km depth. We observe a recovery of the tidal correlation as more events are included. This trend suggests a depth dependence to the tidal correlation, but this trend is not statistically significant. Event depth may influence correlation with the tides because confining pressures increase with depth, so there is a comparatively larger tidal influence at shallow depths. However, tidal stress amplitudes decay with depth, so event depth and tidal stress amplitude are not independent.

On the basis of the earthquake-tide correlation observed, we have tried to estimate the tidal stress amplitude required to trigger an earthquake. We define the percent of excess events, N_{ex}, to be the number of additional or excess events in the tidal phase period with encouraging stress, $N_{ex} = [N_{enc} - (N_{tot}/2)]/N_{tot}$, where N_{enc} is the number of events with $-90° < \theta < 90°$ and N_{tot} is the total number of events. For τ_p greater than 0.02 MPa (0.2 bar), N_{ex} is 24%. This corresponds to 74% of the events (14 of 19 earthquakes) occurring in 50% of the phase time of encouraging stress

($-90° < \theta < 90°$). Successively lower peak tidal stresses show lower tidal correlations, indicating less effective earthquake triggering (Table 2 and Fig. 4B). Standard errors, calculated using data variance, are large because of small numbers of earthquakes in each τ_p bin. In addition to the global data set, 27,464 strike-slip events from California were found to have roughly 1 to 2% more events during times of encouraging tidal stress of <0.004 MPa (Fig. 4B).

A previous study using global data hinted at an earthquake-tide correlation, suggesting that reverse and normal earthquakes correlate either with the shear stress or the trace of the stress tensor J1 (7). In addition, a few regional studies (5, 12–14) in areas with a large ocean-loading component of tidal stress have observed triggering of earthquakes or volcanic tremor. Most often, triggered events have been shallow, normal-type faulting along axial ridges, such as Juan de Fuca (5, 12), perhaps associated with hydrothermal circulation. A recent study of seismicity in Japan showed earthquake-tide

correlation in subregions, with the best correlations found in regions that experienced a large earthquake (15). Our study shows a statistically significant increase in triggering of globally distributed large tectonic events ($M > 5.5$) with increasing tidal stress amplitudes (Fig. 4).

Tidal stress amplitudes required to trigger earthquakes are similar to thresholds suggested for static and dynamic triggering of aftershocks of 0.003 MPa (16–18). A study of triggering after the $M7.4$ Landers event, for example, showed that aftershocks were triggered by stress increases greater than 0.01 MPa (16). In addition, the observed trend of increased triggering with higher imposed tidal stress can be well fit to friction theories of rate- and state-dependent friction and stress corrosion (11, 19, 20).

References and Notes

1. D. Emter, in *Tidal Phenomena*, H. Wilhelm, W. Zurn, H.-G. Wenzel, Eds., vol. 66 of *Lecture Notes in Earth Sciences* (Springer-Verlag, Berlin, 1997), pp. 293–310.
2. S. Hartzell, T. Heaton, *Bull. Seismol. Soc. Am.* **79**, 1282 (1989).
3. J. E. Vidale, D. C. Agnew, M. J. S. Johnston, D. H. Oppenheimer, *J. Geophys. Res.* **103**, 24567 (1998).
4. J. E. Vidale, D. Agnew, D. Oppenheimer, C. Rodriquez, H. Houston, *Eos* **79** (suppl.), F641 (1998).
5. M. Tolstoy, F. L. Vernon, J. A. Orcutt, F. K. Wyatt, *Geology* **30**, 503 (2002).
6. M. O. Saar, M. Manga, *Earth Planet. Sci. Lett.* **214**, 605 (2003).
7. S. Tanaka, M. Ohtake, H. Sato, *J. Geophys. Res.* **107**, 2211 (2002).
8. A. M. Dziewonski, T.-A. Chou, J. H. Woodhouse, *J. Geophys. Res.* **86**, 2825 (1981).
9. The entire data set consists of the 9350 global earthquakes of $M5.5$ or greater from 1977 to 2000 in the Harvard CMT catalog. These events include 2823 reverse, 1040 normal, 3597 strike-slip, and 1890 oblique-type faulting events (7).
10. K. Matsumoto, T. Takanezawa, M. Ooe, *J. Oceanogr.* **56**, 567 (2000).
11. See supporting data on *Science* Online.
12. W. S. D. Wilcock, *Geophys. Res. Lett.* **28**, 3999 (2001).
13. S. Tanaka, M. Ohtake, H. Sato, *Geophys. Res. Lett.* **29**, 10.1029/2002GL015386 (2002).
14. S. I. S. Custodio, J. F. B. D. Fonseca, N. F. d'Oreye, B. V. E. Faria, Z. Bandomo, *Geophys. Res. Lett.* **30**, 1816 (2003).
15. S. Tanaka, M. Ohtake, H. Sato, *Earth Planets Space* **56**, 511 (2004).
16. R. S. Stein, *Nature* **402**, 605 (1999).
17. J. L. Hardebeck, J. J. Nazareth, E. Hauksson, *J. Geophys. Res.* **103**, 24427 (1998).
18. R. S. Stein, *Sci. Am.* **288**, 72 (January 2003).
19. J. H. Dieterich, *Tectonophysics* **144**, 127 (1987).
20. I. Main, *Geophys. J. Int.* **139**, F1 (1999).
21. We thank P. Bird, E. Brodsky, J. Dieterich, H. Houston, D. Jackson, C. Scholz, R. Stein, and three anonymous reviewers for helpful comments and suggestions and K. Matsumoto for making available the ocean tide model NAO.99b. Supported by NSF grant 0125732, an NSF graduate fellowship (E.S.C.), and grant-in-aid for JSPS fellows 07136 (S.T.).